

Machine Learning-Assisted Design and Optimization of Auxetic Structures: A Bioinspired Approach to Mimic Natural Tissues

Masoud Shirzad^a, Morassa Jafari Chashmi^b, Saeideh Khakzadkelarijani^c, Juhyun Kang^d, Mahdi Bodaghi^b, Seung Yun Nam^{a,e,*}

^a Industry 4.0 Convergence Bionics Engineering, Pukyong National University, Busan 48513, Korea

^b Department of Engineering, School of Science and Technology, Nottingham Trent University, Nottingham, NG11 8NS, UK

^c Department of chemical engineering, Pukyong National University, Busan 48513, Korea

^d Department of Biomedical Engineering, Pukyong National University, Busan 48513, Korea

^e Major of Biomedical Engineering, Division of Smart Healthcare, Pukyong National University, Busan 48513, Korea

E-mail: synam@pknu.ac.kr

Keywords: Bioinspired auxetics, Mechanical properties, Tissue engineered scaffolds, Finite element method, Supervised machine learning

Auxetic structures, known for their unique mechanical properties, have gained significant attention across diverse fields. This study designs, manufactures, and optimizes bioinspired auxetic structures for biomedical applications, specifically bone and tendon tissue regeneration. A comparative analysis was conducted to evaluate the compressive and tensile properties of various auxetic designs. All structures were optimized using a cost-effective methodology that integrates the finite element method with data-driven supervised machine learning, maximizing Young's modulus with minimal porosity changes. The findings reveal that design variables significantly influence both auxeticity and mechanical properties. For instance, Young's modulus increased by 135.5% in sharp sinus (SS) and curved sinus (CS) structures while maintaining similar auxeticity. In contrast, the star (St) design showed a 76.5% increase in Young's modulus, with auxeticity increasing from -0.45 to -0.915. The modified re-entrant (M-Re) structure

exhibited higher Poisson's ratio values, closely mimicking cancellous bone. Additionally, structures with higher auxeticity using re-entrant (Re) designs proved suitable for tendon tissue engineering. SS, CS, and St structures offer versatility in achieving a diverse Young's modulus range, making them well-suited for tendon tissue engineering alongside the Re structure.

1. Introduction

Tendon injuries and bone-related disorders are prevalent in modern life, causing severe pain and decreased quality of life ^[1]. Tissue-engineered scaffolds, involving pre-designed porous structures with similar physical and mechanical properties, can serve as a housing for cells to accelerate the healing process of bone and tendon injuries ^[2]. In this regard, utilizing complex bioinspired structures with exceptional properties can be an effective strategy to mimic host tissues ^[3].

Metastructures, including auxetic metastructures, represent a method for fabricating light-weight architectures with unique and multifunctional properties ^[4]. These structures exhibit expansion under tensile loads, indicating a negative Poisson's ratio (NPR) ^[5]. This uncommon behavior leads to high energy absorption ^[6], variable permeability ^[7], improved fracture toughness ^[8], and damage properties of the porous structures ^[9]. Additionally, auxetic structures can isotopically deliver loads to cells and enhance cell proliferation ^[10]. Furthermore, some human tissues, including cancellous bones and tendons, show various levels of auxeticity. The Poisson's ratio can vary near zero for cancellous bones and reach high negative values (approximately -3) for natural tendons ^[11]. Hence, adapting complex auxetic structures can facilitate the biomimicry of human tissue with NPR behaviors ^[12].

Crafting intricate auxetic structures to replicate the characteristics of natural human tissues requires meticulous fabrication techniques. Additive manufacturing, involving the layer-by-layer deposition of materials, is promising for creating these auxetic structures ^[13]. However, after high-precision fabrication using additive manufacturing, an effective evaluation method to accurately assess the mechanical properties of auxetic structures is essential due to their high sensitivity to small structural changes, leading to varied mechanical properties under different conditions ^[14]. Evaluating the mechanical properties of porous auxetic structures is best achieved through experimental methods; however, the cost and time involved in those tests compel researchers to integrate these investigative approaches with computational-based methods. In this context,

computer-aided design (CAD)-based finite element methods (FEM) offer a cost-effective and highly accurate strategy for predicting the mechanical properties of scaffolds [2c, 15]. Moreover, FEM reveals structural deformations and stress distributions, addressing the challenges of a comprehensive evaluation of mechanical hardness [16]. However, determining the optimal design variables using FEM necessitates the creation of multiple CAD models, a process that can be time-intensive [17].

Due to the difficulty of providing various designs, replicating the physical properties, such as Poisson's ratio, of human tissues poses a considerable challenge. Consequently, numerous researchers focus exclusively on identifying mechanical properties akin to those found in human tissues [18]. Nevertheless, the practical implementation of diverse structures to mimic the physical properties of human tissues can prove to be a time-consuming and costly endeavor. In this regard, machine learning (ML) can be beneficial in expediting the optimization of auxetic design variables and programming their properties [19]. These data-driven methods deploy and learn from existing data to make predictions about future outcomes [20]. Additionally, they offer numerous advantages in predicting mechanical properties due to their high adaptability to various designs, independence from specific physical designs, and lower computational costs compared to relying solely on FEM [21]. In accordance with these positive impacts, researchers have employed various ML methods to predict the mechanical properties of porous structures, including auxetic architectures [19b, 22].

To address the gap pertaining to the consideration of various physical and mechanical properties of scaffolds, this study implements ML methods to comprehensively investigate five distinct bioinspired auxetic structures and predict their corresponding Young's modulus. The study also aims to enhance Young's modulus within these designs while minimizing alterations to porosity levels and aligning with the auxeticity observed in human bone and tendon tissues. As presented in Figure 1, multiple bioinspired and conventional structures were designed using CAD software and meticulously fabricated by additive manufacturing techniques. Subsequently, the mechanical properties of the auxetic structures underwent rigorous examination through experimental methods. To facilitate data-driven ML approaches, design variables for each structure were systematically modified and mechanically evaluated using FEM simulation. Ultimately, the optimal structures were predicted by an ML technique and manufactured, and their performances were

experimentally verified based on the ML results. This study demonstrates the potential of machine learning in advancing the fabrication of bioinspired auxetic structures for biomedical applications.

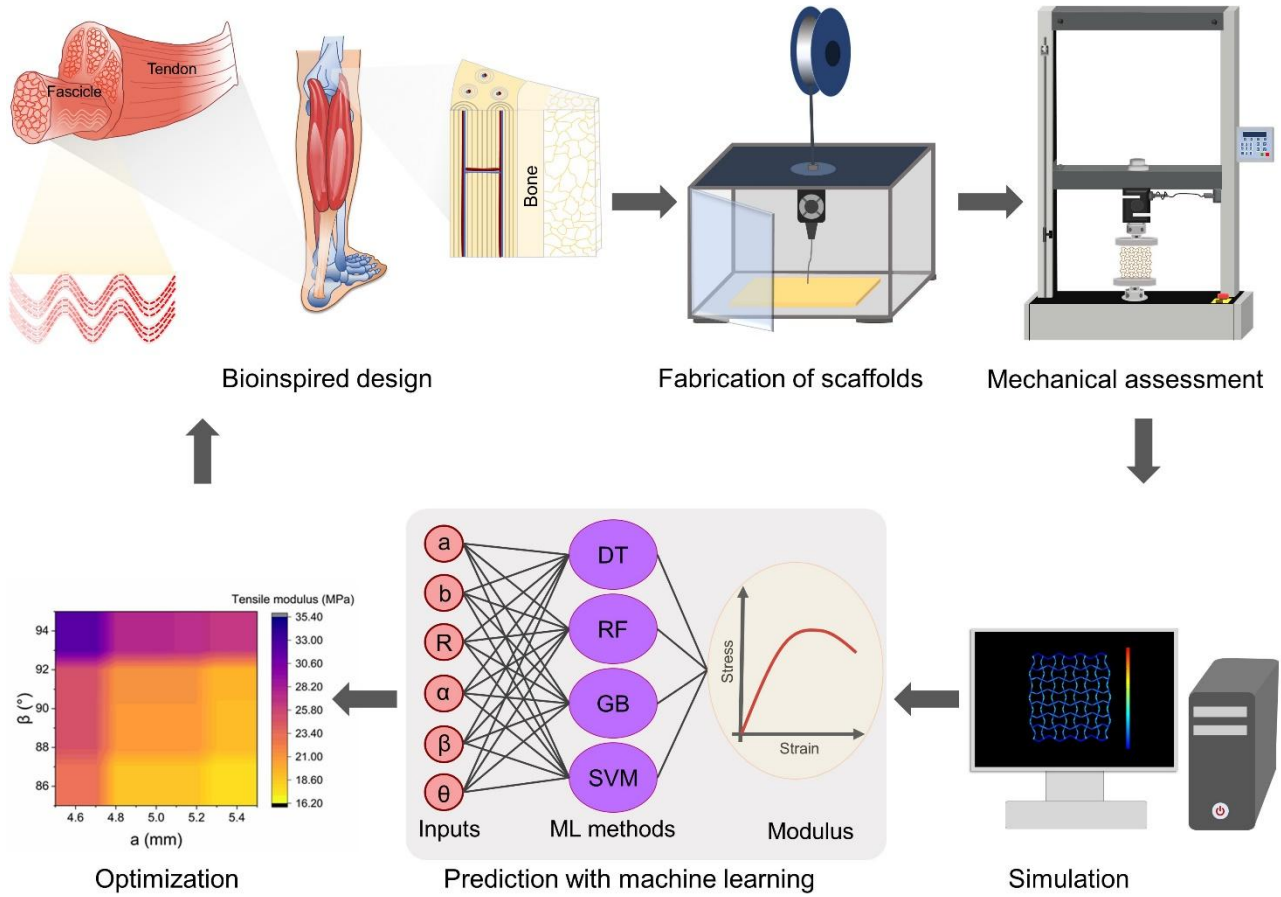


Figure 1. Overview of the process of design, fabrication, and evaluation of auxetic structures.

2. Results

2.1. Assessment of mechanical properties

For clarity and consistency, the following abbreviations are used throughout this study: re-entrant (Re), modified re-entrant (M-Re), sharp sinus (SS), curved sinus (CS), star (St), decision tree (DT), random forest (RF), gradient boosting (GB), support vector machine (SVM), normalized mean square error (NMSE), mean squared error (MSE), coefficient of determination (R^2), and cross-validation (CV). To curate a dataset for data-driven methodologies, variables were systematically adjusted, guided by the insights from Table 2 and Table 5, with a focus on minimizing alterations to the porosity of scaffolds. Subsequently, the newly devised structures underwent rigorous scrutiny by FEM to quantify the Young's modulus. Each of these procedural stages is meticulously

delineated in Figure 2, Table 1, and Table 2. Furthermore, the printing resolution of the auxetic structures and the differences between the designed and measured porosity are presented in Table S21. These results confirm the reliable quality of the printed auxetic structures in this study.

Consequently, distinct sets of designs—42 for Re, 42 for M-Re, 27 for SS, 81 for CS, and 72 for St structures—were generated. The mechanical analysis of all structures under both tensile and compressive loads is graphically represented in Figure 3 and Figure S1. Details of physical variables and Young's modulus are presented in Table S1-S5.

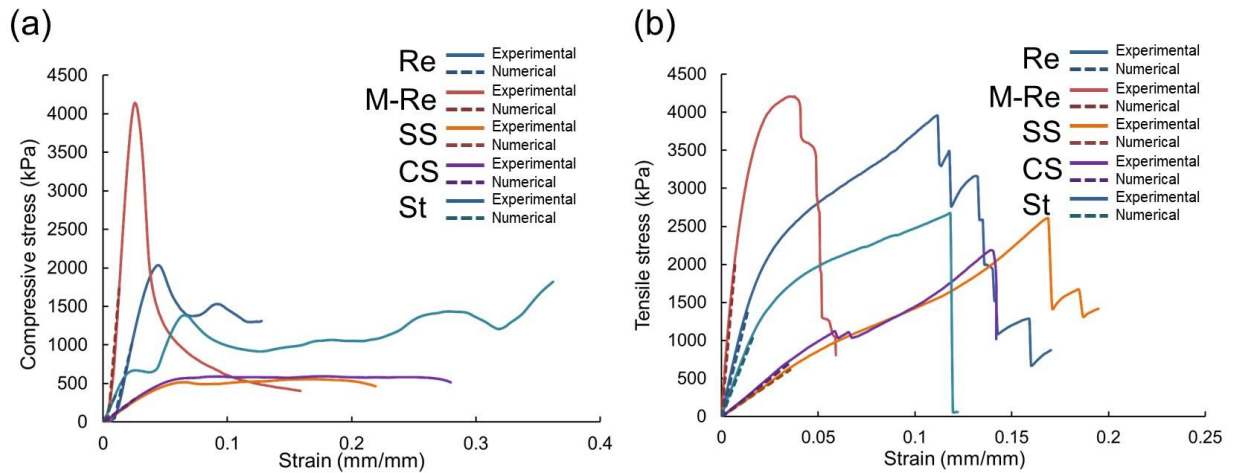


Figure 2. (a) Compressive mechanical properties and (b) tensile mechanical properties of auxetic structures and their numerical validations.

Table 1. Experimental and numerical values of Young's modulus, porosities, and Poisson's ratio of different auxetic structures.

Structure	Experimental compressive modulus (MPa)	Experimental tensile modulus (MPa)	Numerical compressive modulus (MPa)	Numerical tensile modulus (MPa)	Porosity (%)	Poisson's ratio
Re	84.23	106.19	83.15	103.05	71.89	-1.632
M-Re	243.32	279.31	242.53	286.18	70.19	-0.684
SS	10.54	17.23	10.76	17.62	81.3	-1.11
CS	12.74	19.06	13.1	19.85	80.8	-1.05
St	35.41	66.12	35.09	66.91	70.5	-0.45

Table 2. Variables of the design of different auxetic structures and their intervals.

Structure	a (mm)	b (mm)	R (mm)	α (°)	β (°)	θ (°)	Porosity (%)
Re	7-9	4-5	-	55-65	-	-	64.29 - 77.12
M-Re	7-9	4-5	-	55-65	-	-	65.36 - 76.24
SS	4.5-5.5	-	-	20-30	85-95	-	75.5 - 83.07
CS	4.5-5.5	-	2.5-3.5	20-30	85-95	-	76.24 - 82.92
St	4-5	-	-	20-30	85-95	30-40	65.31 - 76.42

2.2. Machine learning performance

The performance of machine learning models was assessed through the calculation of the MSE, NMSE, and R^2 using Equation 4, 5 and 6. The best model for each dataset was selected based on the lowest values of the MSE and NMSE, and the highest value of the R^2 . Figure 4, Table 3, and Table S6-S20 illustrates the training of all datasets using four distinct ML methods, aiming to determine the optimal ML approach for predicting mechanical properties. A lower MSE and NMSE, along with higher R^2 value, signifies superior learning performance. Furthermore, hyperparameters were meticulously tuned with MSE, NMSE, and R^2 as evaluation metrics. The details of this selection process are provided in Table S6-S20. It is worth noting that the ratio of splitting a dataset into training and testing datasets can extensively affect the performance of the prediction of a machine learning model^[23]. Accordingly, three distinct training test size ratios (0.1, 0.2, and 0.3) and two cross-validation (CV) values were examined. This procedure can extensively improve predictions. For example, NMSE decreased from 3.703 in DT to 0.244 with the SVM model in the M-Re structure under tensile load. To deepen the scrutiny of the best models, an analysis of the correlation between predicted and actual Young's moduli was conducted and presented in Figure 5. The best ML models for each dataset were selected based on the prediction accuracy, and those models were implemented to predict Young's modulus.

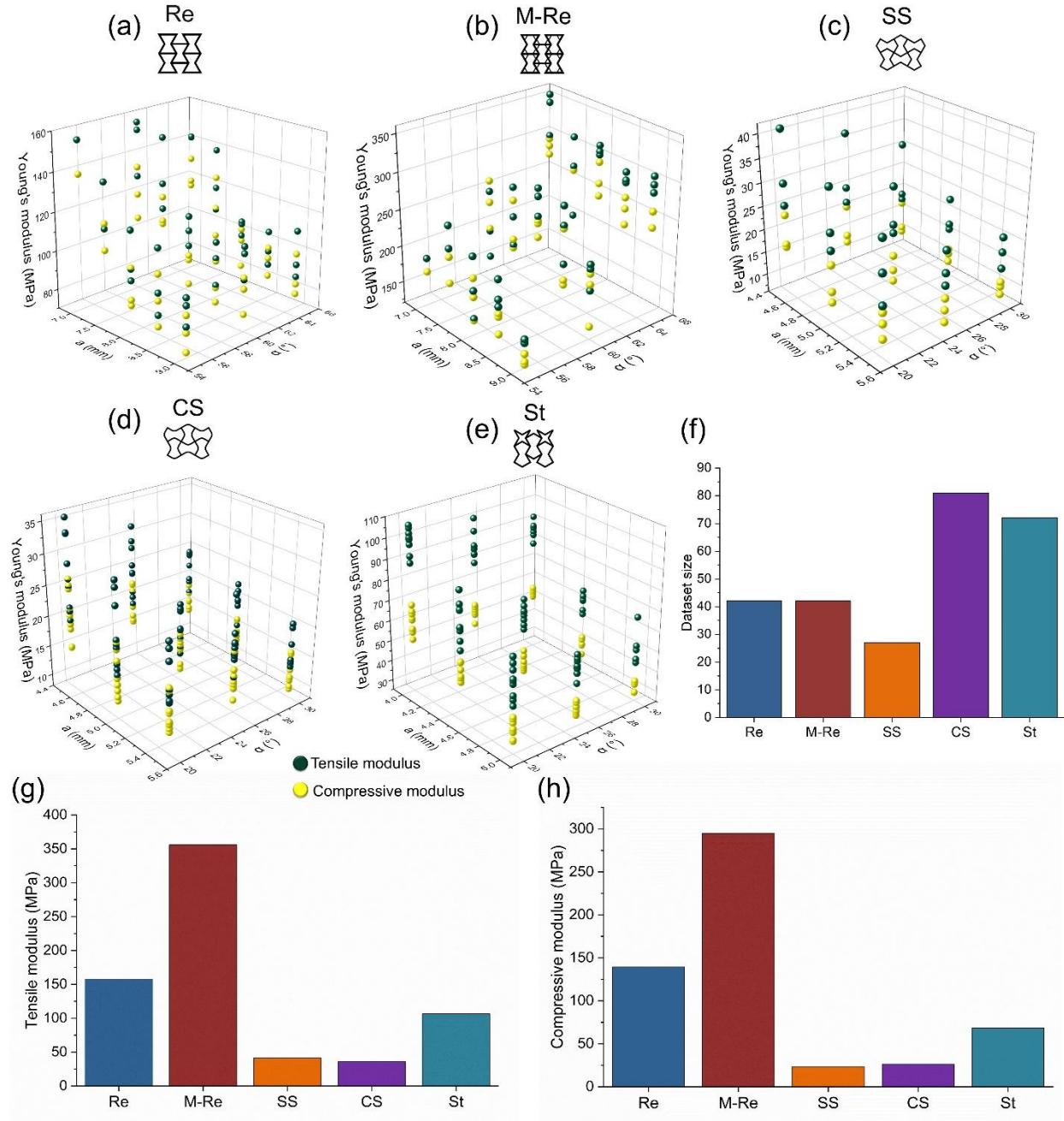


Figure 3. Investigation of the mechanical properties of different auxetic designs with FEM: (a) Re, (b) M-Re, (c) SS, (d) CS, and (e) St structures with different (f) dataset sizes. (g) Maximum tensile and (h) compressive mechanical properties of auxetic structures.

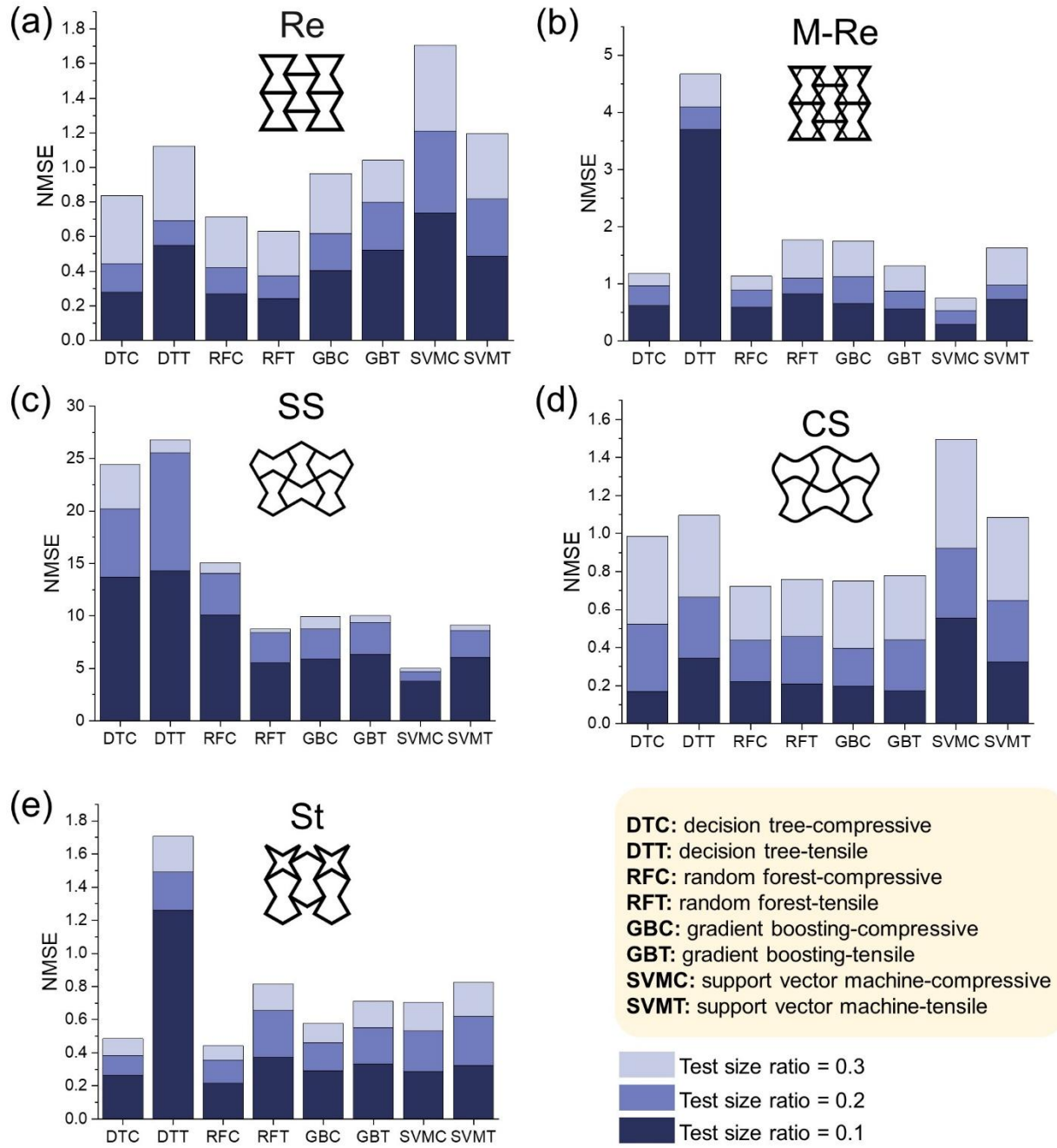


Figure 4. ML performance of (a) Re, (b) M-Re, (c) SS, (d) CS, and (e) St structures based on the NMSE.

Table 3. Selection of the best ML models for different structures.

	Structure	Best ML model	Test size ratio	CV	NMSE
Re	Compressive	RF	0.2	5	0.152
	Tensile	RF	0.2	5	0.131
M-Re	Compressive	SVM	0.3	5	0.212
	Tensile	SVM	0.2	5	0.244
SS	Compressive	SVM	0.3	5	0.278
	Tensile	RF	0.3	5	0.334
CS	Compressive	DT	0.1	5	0.170
	Tensile	GB	0.1	5	0.171
St	Compressive	RF	0.3	5	0.0875
	Tensile	RF	0.3	5	0.162

2.3. Predictions by ML models

The mechanical properties of all auxetic structures can be investigated by experimental and numerical methods. However, sequential processes, including designing, fabricating, and FEM evaluating the porous auxetic structures, can be time-consuming and costly. In this regard, supervised ML methods were used to precisely predict the mechanical properties of scaffolds. Figure 6a-e illustrate predictions of the mechanical properties of auxetic structures based on ML methods, accompanied by experimentally calculated mechanical properties of auxetic structures as presented in Figure 6f and 6g. Figure 6a-e and Figure S2-S6 are displayed to analyze the dependency of the mechanical properties and physical variables of scaffolds. Based on the ML optimization, specific structures with the highest Young's modulus were selected to fabricate and verify using experimental results.

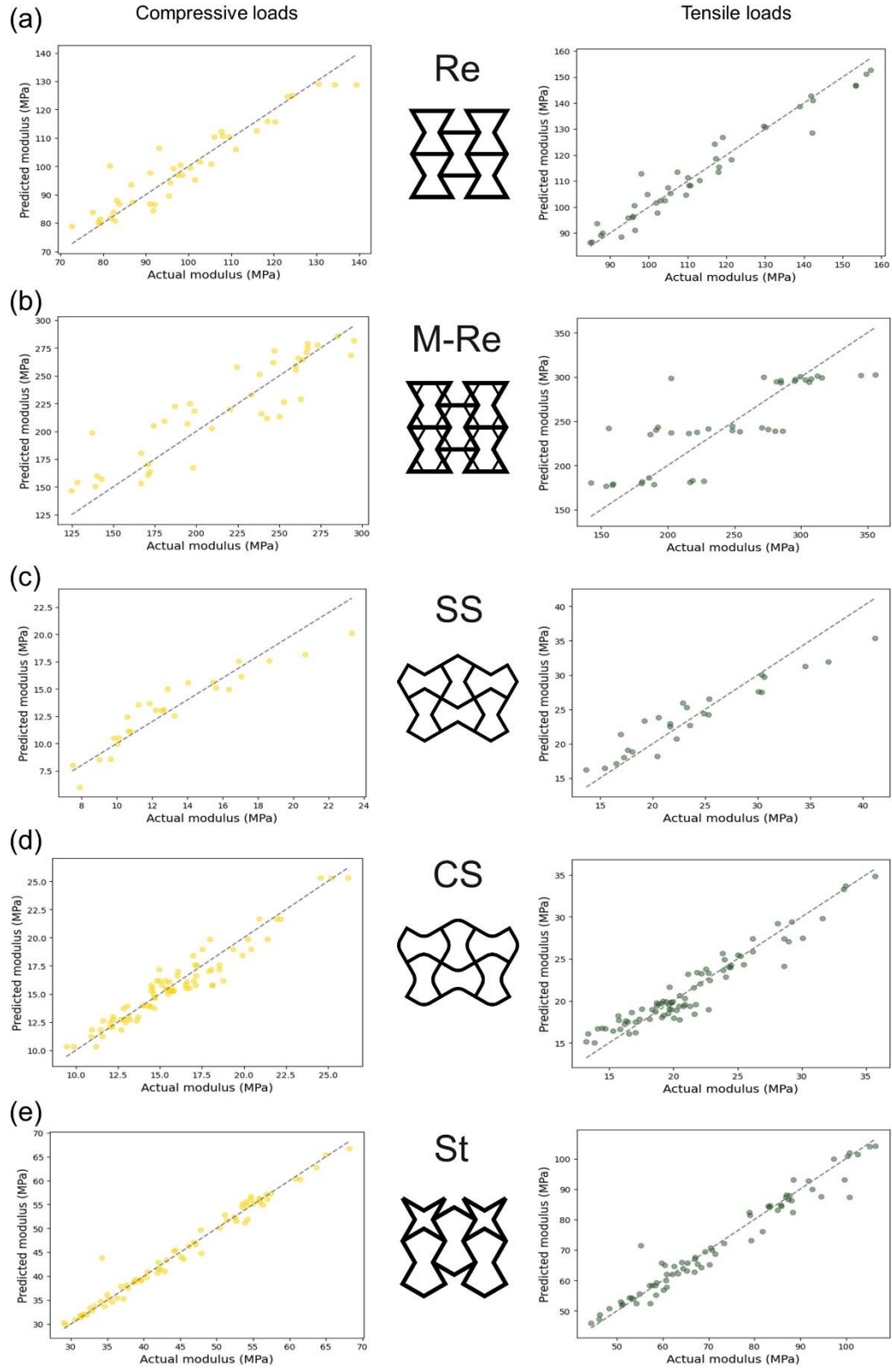


Figure 5. Fitting actual values with prediction values for (a) Re, (b) M-Re, (c) SS, (d) CS, and (e) St structures.

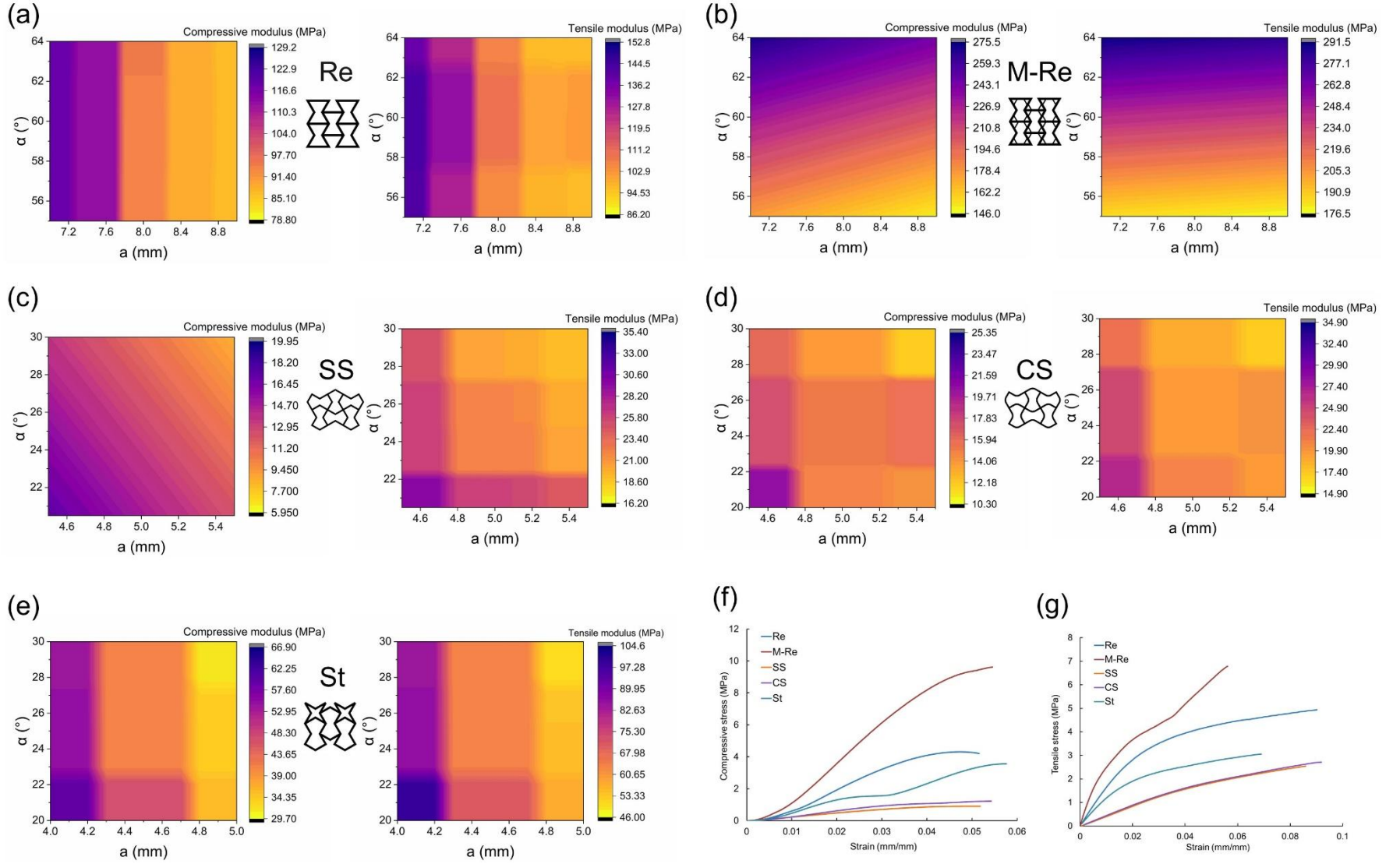


Figure 6. ML predictions of Young's modulus of (a) Re, (b) M-Re, (c) SS, (d) CS, and (e) St structures under compressive and tensile loads. Experimental mechanical properties of optimized auxetic structures under (f) compressive and (g) tensile loads.

2.4. Fabrication of optimized structures

To demonstrate the accuracy of the method presented in this study, all optimized structures were fabricated and tested under the same conditions. The results of the optimized structures are illustrated in Figure 6f-g, Figure 7, and Table 4. Figure 6f-g show the experimental investigation of optimized structures elaborated in Table 4. In the Table 4, besides the physical variables, numerical predictions of the mechanical properties are provided for comparison of the results. The results exhibited that the error can fall within an acceptable interval between 0.4% and 10.7%, which shows the reliability of the present method.

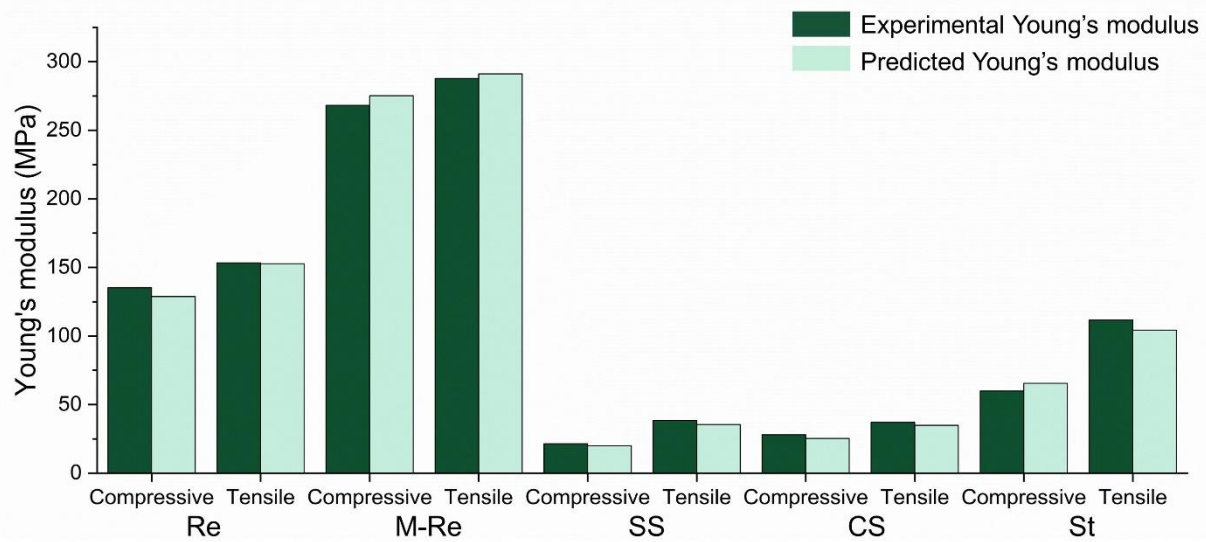
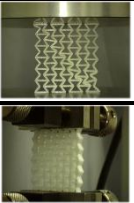
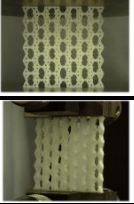
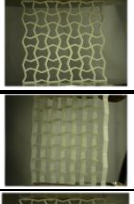
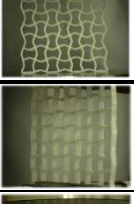
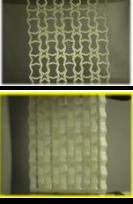


Figure 7. Experimental and ML predicted mechanical properties of auxetic scaffolds under compressive and tensile loads.

Table 4. Physical and mechanical properties of different optimized auxetic structures.

Structure	Loading condition	a (mm)	b (mm)	R (mm)	α (°)	β (°)	θ (°)	Experimental Young's modulus (MPa)	Predicted Young's modulus (MPa)	Error of prediction (%)	Porosity (%)	Poisson's ratio
Re		7	4	-	60	-	-	135.23	128.75	5%	65.29	-1.219
								153.33	152.67	0.4%		
M-Re		7	4	-	65	-	-	268.21	275.19	2.5%	68.77	-0.115
								287.82	291.08	1.1%		
SS		4.5	-	-	20	95	-	21.43	19.95	7.4%	76.84	-1.081
								38.43	35.37	8.6%		
CS		4.5	-	3.5	20	95	-	28.04	25.31	10.7%	75.56	-1.011
								37.17	34.82	6.7%		
St		4	-	-	20	90	30	59.96	65.43	8.3%	72.79	-0.915
								111.63	104.22	7.1%		

3. Discussion

This study undertakes a comparative analysis and optimization of five distinct auxetic structures for potential emulation and utilization in biomedical engineering applications. Specifically, the investigation aims to replicate the physical and mechanical properties of bone and tendon tissues, encompassing a broad spectrum of auxeticity in scaffold design. These five structures were selected to represent a diverse range of geometries and Poisson's ratio behaviors, enabling the design of scaffolds tailored to the mechanical demands of various tissues, while also ensuring compatibility with 3D printing and computational modeling constraints. From a physical perspective, auxetic structures enable control over Poisson's ratio to meet specific biomechanical requirements—such as achieving near-zero Poisson's ratio for cancellous bone or higher auxeticity in tendon tissues [5a, 11b]. Previous studies have also highlighted the positive effects of NPR structures on cell growth and attachment, compared to conventional structures with a positive Poisson's ratio [5a, 10, 24]. Moreover, FEM was employed to generate data for data-driven approaches, offering the potential to reduce both the cost and time associated with scaffold fabrication and experimental investigation of mechanical properties. As illustrated in Figures 2, Table 1, and Figure 3, a singular experimentally fabricated structure suffices to initiate a data-driven methodology, as it can be complemented by FEM to augment the dataset. It should be noted that using only experimental or FEM approach cannot provide a deep understanding of the relation between physical variables and mechanical properties [2c, 13a, 25].

In the Re structure, Young's modulus was increased by 65% and 44% under compression and tension, respectively. The porosity decreased by 6.6%, but the Poisson's ratio increased by 25%. These results show the dependency of the Re structures on Poisson's ratio. With a higher NPR, Young's modulus would increase extensively. This trend is counteracted by increased bending deformation in structures with higher NPR, which can lead to a reduction in overall modulus [26]. However, in the M-Re structure, the Poisson's ratio has almost no effect on the mechanical properties of scaffolds. This phenomenon can be explained by controlling the moment by adding inclined struts to the basic Re structure. The small inclined struts in M-Re can control the rotation under tensile and compression loads, allowing for better manipulation of stress in M-Re scaffolds and decreasing local stress [2c]. Additionally, previous study illustrated that M-Re structure has higher capability of the stress distribution compared to Re structure [2c]. On the other hand, SS and

CS structures, which feature more inclined struts in their unit cells, increased the complexity of the load-bearing behavior of these structures compared to the Re and M-Re architectures. Specifically, the mechanical properties in SS and CS structures improved by up to 135.5%, with almost no change in Poisson's ratio and around a 5% decrease in porosity. Comparing SS and CS structures clarified that adding curvature to the struts of auxetic structures does not extensively change the physical and mechanical properties in auxetic designs. The results imply that complex structures require a comprehensive optimization method to improve their mechanical properties. This conclusion was consistently valid for the St structure as well. In this design, the compressive and tensile moduli improved by 64% and 76.5%, respectively, with an increase of 2.29% in porosity. The Poisson's ratio significantly decreased from -0.45 to -0.915 in the St optimized design, showing the importance of optimization in complex auxetic structures. From the perspective of machine learning, the relationship between the testing and training data ratios is influenced by the distribution of mechanical outcomes. In computational simulations, the distribution of Young's modulus in CS structure does not adhere to a consistent pattern, unlike in other designs. Consequently, a higher proportion of training data is necessary to accurately predict the mechanical properties of these structures, as illustrated in Figure 3d, Table 3, and Figure 6d.

Among all five structures, the M-Re structure exhibits the highest values for both Poisson's ratio and Young's modulus. Its optimized structure, characterized by a high Poisson's ratio (lowest absolute value), proves to be a suitable choice for applications in bone tissue engineering ^[2c, 11a]. Young's modulus of human cancellous bone typically falls within the normal range of 10 MPa to 2 GPa with a near-zero Poisson's ratio. The optimized M-Re structure demonstrates favorable Young's modulus, Poisson's ratio, and porosity, further supporting its appropriateness for bone tissue engineering ^[2c, 11a, 27]. The mechanical properties of tendons are intricate and vary with factors such as gender, body mass, and age. Despite this complexity, tendons can exhibit a high level of auxeticity. For instance, Young's modulus of the Achilles tendon can range from 2.0 ± 0.4 GPa to 140.5 ± 29.3 MPa with a Poisson's ratio falling between -0.39 and -3 ^[11b, 28]. Consequently, Re, SS, CS, and St structures can be employed in different study cases due to their coverage of diverse Poisson's ratios and mechanical properties. In addition to these static characteristics, dynamic performance is also a critical factor in scaffold design. For example, our previous study confirmed the suitability of the St structure under dynamic tensile loading. A future direction could

involve conducting dynamic studies using larger datasets ^[29]. Another promising approach is the inverse design of auxetic structures for tendon and bone implants, which could further enhance their performance and better mimic the mechanical behavior of native tissues. Overall, the results of this study can be applied to cases with a wide range of auxeticity and Young's modulus, coupled with high porosity, which is suitable for applications in both tendon and bone tissue engineering.

4. Conclusion

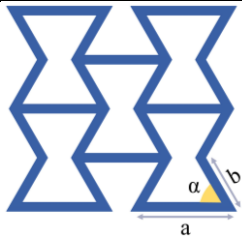
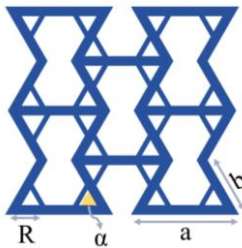
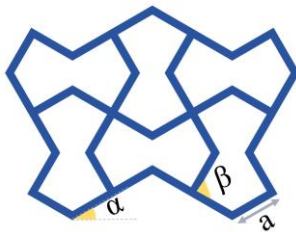
This study used five different auxetic designs with four various machine learning methods to predict and optimize elastic modulus of these NPR structures. In this low-cost method, FEM and ML approaches were employed to predict the mechanical properties of auxetic designs under tension and compression. The results affirmed that the presented methodology effectively predicted the mechanical properties of porous scaffolds with minimal error. Furthermore, Young's modulus could be enhanced by up to 135.5% with slight adjustments in porosity. Moreover, the findings indicated that various auxetic structures could show different responses when changing the variables of the design. For instance, auxeticity could significantly affect mechanical properties in Re and St designs, whereas it did not extensively change the mechanical properties of SS, CS, and M-Re structures. In conclusion, designing various auxetic structures could cover a wide range of auxeticity and mechanical properties, improving the accuracy of choosing appropriate architectures with a low-cost method to mimic the physical and mechanical properties of human tissues, such as bone and tendons.

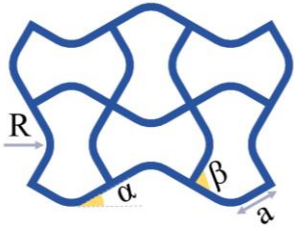
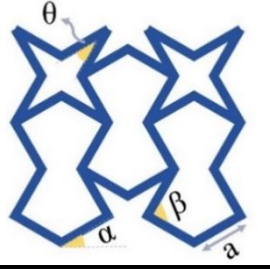
5. Experimental Methods

5.1. Designing and fabrication of scaffolds: Five distinct structures were conceived based on mimicking human tissues. The structures for all five designs were generated using 3D CAD software (SolidWorks, Dassault Systèmes). These initial designs were diversified into combinations of variables to comprehensively investigate mechanical properties and furnish outcomes for data-driven approaches (refer to Supplementary Materials); however, physical properties such as porosity exhibited minimal variation. Table 5 presents a visual representation of the auxetic structures, re-entrant (Re), modified re-entrant (M-Re), sharp sinus (SS), curved

sinus (CS), and star (St), and their respective dimensions. It should be noted that the depth of all samples is equal to 5 mm. Subsequently, the CAD models were converted to STL file format for fabrication using a 3D printer (3DWOX 1, Sindoh) based on fused deposition modeling (FDM) and polylactic acid (PLA) filaments, which have been widely used for biomedical applications. Furthermore, the following parameters were considered as the printing parameters: nozzle temperature: 200 °C, bed temperature: 60 °C, layer height: 0.2 mm, print speed: 10 mm/s, infill density: 100%, and nozzle diameter: 0.4 mm. To ensure the consistency, all parameters were kept same. Additionally, the present study aimed to encompass a broad spectrum of auxeticity, intending applicability for both bone and tendon scenarios. The thickness of all the struts in auxetic designs is equal to 0.8 mm except M-Re, which has a hierarchical structure with 0.8 mm and 0.4 mm struts. The printing quality and the differences between the designed and fabricated structures are illustrated in Table S21.

Table 5. Initial designs of auxetic structures and their dimensions.

Structures	Designs	a (mm)	b (mm)	R (mm)	α (°)	β (°)	θ (°)
Re-entrant (Re)		8	5	-	60	-	-
Modified re-entrant (M-Re)		8	5	3	60	-	-
Sharp sinus (SS)		5	-	-	30	90	-

Curved sinus (CS)		5	-	3	30	90	-
Star (St)		5	-	-	30	90	30

Assessment of mechanical properties: According to ASTM D695 and ASTM D638, two bulk samples (cylindrical and dog-bone-shaped) were fabricated for utilization in the FEM simulation (Figure S7). The compression and tensile properties of both bulk and porous auxetic structures were assessed using a universal testing machine (LR5K plus, LLOYD Instruments) equipped with a 5 kN load cell. Additionally, a speed of 1 mm/min was set for the head of the universal testing machine to ensure quasi-static behavior in all samples. The height of the samples was decreased or increased by at least 20% to obtain the stress-strain curve of the samples. Three of each structure were fabricated and tested to validate the experimental mechanical outcomes. Additionally, the calculation of the Poisson's ratio was based on previous studies ^[2c, 29]. Briefly, a camera was used to capture images, which were then analyzed using ImageJ software. Subsequently, the following formulas were utilized to calculate Poisson's ratio (ν_{xy}). In the following equations, ϵ_x and ϵ_y represent the strains in the X and Y directions, respectively; Δ_x and Δ_y denote the deformations in the X and Y directions; and l_x and l_y refer to the initial distances between reference points in the X and Y directions, respectively.

$$\epsilon_x = \frac{\Delta_x}{l_{x0}} \quad (1)$$

$$\epsilon_y = \frac{\Delta_y}{l_{y0}} \quad (2)$$

$$\nu_{xy} = -\frac{\epsilon_x}{\epsilon_y} \quad (3)$$

FEM simulations: COMSOL Multiphysics FEM software (COMSOL Inc.) was employed for a thorough exploration of the mechanical properties of auxetic structures, incorporating various variables to generate a dataset for data-driven approaches. Additionally, the following parameters and linear solver were considered for the constitutive material properties in the FEM study: compressive modulus, tensile modulus, Poisson's ratio, and density, which were 1025 MPa, 1236 MPa, 0.28, and 1.25 g/cm³, respectively. The primary objective was to establish a comprehensive dataset suitable for subsequent data-driven analyses. In the initial phase, once CAD models were imported into the FEM software, boundary conditions, mirroring real-world scenarios (fully constrained on one side and loaded on the opposite side), were systematically applied to each design. Subsequently, a 3D tetrahedral element was selected based on scaffold structures to mesh the 3D auxetic architectures. A sensitivity analysis was conducted to ascertain the optimal number of elements.

Machine learning optimization: Four distinct machine learning models, namely decision tree (DT), random forest (RF), gradient boosting (GB), and support vector machine (SVM), were employed for training and predicting across ten diverse datasets. This study aimed to explore the effectiveness of different machine learning methods by employing various input variables and assessing their performance across the ten distinct datasets within the scope of this research.

The DT algorithm is extensively employed in the supervised exploration of scientific inquiries. This methodology initiates from a parent (root) node and progressively divides into two nodes, continuing this process until the nodes reach an endpoint where further division is no longer feasible ^[30]. In the RF method, multiple decision trees are amalgamated to form a forest-like structure. Within this algorithm, the regressor computes the average of the outputs from different trees within the entire forest ^[31]. Moreover, the GB algorithm combines multiple base classifiers to enhance their performance, and it employs a gradient descent method to solve a minimization problem ^[32]. In addition, SVM establishes a non-linear relationship between inputs and outputs, seeking to identify a hyperplane within an N-dimensional space where an N-number of features can be considered for classification ^[33]. GridSearchCV in the Scikit-Learn toolkit in Python was employed to fine-tune the hyperparameters of the machine learning methods ^[20a]. Given the utilization of diverse datasets, the accuracy of all predictions was assessed using the mean square

error (MSE), normalized mean square error (NMSE), and coefficient of determination (R^2), calculated with the following formula:

$$MSE = \frac{1}{n} \sum_{i=1}^n (Y_i - \hat{Y}_i)^2 \quad (4)$$

$$NMSE = \frac{\sum_{i=1}^n (Y_i - \hat{Y}_i)^2}{\sum_{i=1}^n (Y_i - \bar{Y})^2} \quad (5)$$

$$R^2 = 1 - NMSE \quad (6)$$

where n , Y_i , \hat{Y}_i , and \bar{Y} are the number of observations, the observed value for the i -th observation, the predicted value for the i -th observation, and the mean of the observed values, respectively.

Details of the GridSearchCV for tuning the hyperparameters are mentioned below.

Decision tree:

maximum depth of the tree: [None, 10, 20, 30]

minimum number of samples required to split an internal node: [2, 5, 10]

minimum number of samples required to be at a leaf node: [1, 2, 4]

random forest:

number of estimators: [50, 100, 150, 200]

maximum tree depth: [None, 10, 20, 30]

minimum samples required to split an internal node: [2, 5, 10]

minimum samples required to be at a leaf node: [1, 2, 4]

gradient boosting:

number of boosting stages: [50, 100, 150, 200]

step size shrinkage: [0.01, 0.05, 0.1, 0.2]

maximum depth of individual regression estimators: [3, 4, 5, 6]

minimum number of samples required to split an internal node: [2, 5, 10]

support vector machine:

regularization parameter: [0.1, 1, 10]

epsilon: [0.1, 0.2, 0.5]

kernel function: [linear, radial basis function, polynomial]

Acknowledgment

This research was supported by a National Research Foundation of Korea (NRF) grant (NRF-2021R1I1A3040459) funded by the Korean government (MOE). This research was supported by a grant of the Korea Health Technology R&D Project through the Korea Health Industry Development Institute (KHIDI), funded by the Ministry of Health & Welfare, Republic of Korea (grant number: HI22C1323).

References

- [1] a) M. Alonzo, F. A. Primo, S. A. Kumar, J. A. Mudloff, E. Dominguez, G. Fregoso, N. Ortiz, W. M. Weiss, B. Joddar, Bone tissue engineering techniques, advances, and scaffolds for treatment of bone defects, *Current opinion in biomedical engineering* **2021**, 17, 100248; b) J. Zhang, X. Zhu, S. Chen, P. Li, L. Yang, J. Zhang, The research status of biodegradable polymers in repair of Achilles tendon defects, *International Journal of Polymeric Materials and Polymeric Biomaterials* **2023**, 1; c) Y. H. Son, D. H. Yang, B. Uricoli, S.-J. Park, G.-J. Jeong, H. J. Chun, Three-dimensional cell culture system for tendon tissue engineering, *Tissue Engineering and Regenerative Medicine* **2023**, 20, 553.
- [2] a) M. M. Zerankeshi, R. Bakhshi, R. Alizadeh, Polymer/metal composite 3D porous bone tissue engineering scaffolds fabricated by additive manufacturing techniques: A review, *Bioprinting* **2022**, 25, e00191; b) E.-S. Motiee, S. Karbasi, E. Bidram, M. Sheikholeslam, Investigation of physical, mechanical and biological properties of polyhydroxybutyrate-chitosan/graphene oxide nanocomposite scaffolds for bone tissue engineering applications, *International journal of biological macromolecules* **2023**, 247, 125593; c) M. Shirzad, M. Bodaghi, D. Oh, M. Yi, S. Y. Nam, Design and optimization of bioinspired auxetic structure for biomedical applications, *European Journal of Mechanics-A/Solids* **2024**, 103, 105139.
- [3] T. Li, J. Chang, Y. Zhu, C. Wu, 3D printing of bioinspired biomaterials for tissue regeneration, *Advanced healthcare materials* **2020**, 9, 2000208.
- [4] S. Bronder, F. Herter, A. Röhrig, D. Bähre, A. Jung, Design study for multifunctional 3D re-entrant auxetics, *Advanced Engineering Materials* **2022**, 24, 2100816.
- [5] a) M. Shirzad, A. Zolfagharian, M. Bodaghi, S. Y. Nam, Auxetic metamaterials for bone-implanted medical devices: Recent advances and new perspectives, *European Journal of Mechanics-A/Solids* **2022**, 104905; b) Y. Kim, K. H. Son, J. W. Lee, Auxetic structures for tissue engineering scaffolds and biomedical devices, *Materials* **2021**, 14, 6821; c) Y. Yao, H. Yuan, H. Huang, J. Liu, L.

- Wang, Y. Fan, Biomechanical design and analysis of auxetic pedicle screw to resist loosening, *Computers in Biology and Medicine* **2021**, 133, 104386.
- [6] a) R. Hamzehei, M. Bodaghi, N. Wu, 3D-printed highly stretchable curvy sandwich metamaterials with superior fracture resistance and energy absorption, *International Journal of Solids and Structures* **2023**, 112570; b) X. C. Teng, X. Ren, Y. Zhang, W. Jiang, Y. Pan, X. G. Zhang, X. Y. Zhang, Y. M. Xie, A simple 3D re-entrant auxetic metamaterial with enhanced energy absorption, *International Journal of Mechanical Sciences* **2022**, 229, 107524.
- [7] A. Alderson, J. Rasburn, K. Evans, J. Grima, Auxetic polymeric filters display enhanced de-fouling and pressure compensation properties, *Membrane Technology* **2001**, 2001, 6.
- [8] X. Li, Q. Wang, Z. Yang, Z. Lu, Novel auxetic structures with enhanced mechanical properties, *Extreme Mechanics Letters* **2019**, 27, 59.
- [9] A. C. Kaya, A. Korucu, M. Boğuşlu, Influence of additional strut elements in 3D Re-Entrant auxetic unit cells on the damage and energy absorption properties, *Experimental Mechanics* **2024**, 64, 639.
- [10] M. J. Kim, H. J. Choi, J. Cho, J. B. Lee, H.-J. Sung, J. K. Kim, MG-63 cell proliferation with static or dynamic compressive stimulation on an auxetic PLGA scaffold, *International Journal of Polymer Science* **2017**, 2017.
- [11] a) J. Williams, J. Lewis, Properties and an anisotropic model of cancellous bone from the proximal tibial epiphysis, **1982**; b) R. Gatt, M. V. Wood, A. Gatt, F. Zarb, C. Formosa, K. M. Azzopardi, A. Casha, T. P. Agius, P. Schembri-Wismayer, L. Attard, Negative Poisson's ratios in tendons: an unexpected mechanical response, *Acta biomaterialia* **2015**, 24, 201.
- [12] R. Hedayati, A. Yousefi, M. L. Dezaki, M. Bodaghi, Analytical relationships for 2D Re-entrant auxetic metamaterials: An application to 3D printing flexible implants, *Journal of the mechanical behavior of biomedical materials* **2023**, 143, 105938.
- [13] a) M. Shirzad, A. Zolfagharian, A. Matbouei, M. Bodaghi, Design, evaluation, and optimization of 3D printed truss scaffolds for bone tissue engineering, *Journal of the mechanical behavior of biomedical materials* **2021**, 120, 104594; b) C. T. Wanniarachchi, A. Arjunan, A. Baroutaji, M. Singh, Mechanical performance of additively manufactured cobalt-chromium-molybdenum auxetic meta-biomaterial bone scaffolds, *Journal of the mechanical behavior of biomedical materials* **2022**, 134, 105409; c) S. Wang, Y. Ma, Z. Deng, S. Zhang, J. Cai, Effects of fused deposition modeling process parameters on tensile, dynamic mechanical properties of 3D printed polylactic acid materials, *Polymer Testing* **2020**, 86, 106483.
- [14] H. Kolken, K. Lietaert, T. van der Sloten, B. Pouran, A. Meynen, G. Van Loock, H. Weinans, L. Scheys, A. A. Zadpoor, Mechanical performance of auxetic meta-biomaterials, *Journal of the mechanical behavior of biomedical materials* **2020**, 104, 103658.
- [15] a) A. B. Kakarla, I. Kong, S. G. Nukala, W. Kong, Mechanical behaviour evaluation of porous scaffold for tissue-engineering applications using finite element analysis, *Journal of Composites Science* **2022**, 6, 46; b) S. S. Mohol, M. Kumar, V. Sharma, PLA-based nature-inspired architecture for bone scaffolds: A finite element analysis, *Computers in Biology and Medicine* **2023**, 163, 107163.
- [16] Y.-G. Koh, J.-A. Lee, Y. S. Kim, H. Y. Lee, H. J. Kim, K.-T. Kang, Optimal mechanical properties of a scaffold for cartilage regeneration using finite element analysis, *Journal of tissue engineering* **2019**, 10, 2041731419832133.
- [17] J. Peloquin, A. Kirillova, C. Rudin, L. Brinson, K. Gall, Prediction of tensile performance for 3D printed photopolymer gyroid lattices using structural porosity, base material properties, and machine learning, *Materials & Design* **2023**, 232, 112126.
- [18] a) R. Owen, C. Sherborne, T. Paterson, N. H. Green, G. C. Reilly, F. Claeyssens, Emulsion templated scaffolds with tunable mechanical properties for bone tissue engineering, *Journal of*

- the mechanical behavior of biomedical materials* **2016**, 54, 159; b) R. Baptista, M. Guedes, Porosity and pore design influence on fatigue behavior of 3D printed scaffolds for trabecular bone replacement, *Journal of the mechanical behavior of biomedical materials* **2021**, 117, 104378.
- [19] a) A. Clausen, F. Wang, J. S. Jensen, O. Sigmund, J. A. Lewis, Topology optimized architectures with programmable Poisson's ratio over large deformations, *Advanced Materials* **2015**, 27, 5523; b) J. K. Wilt, C. Yang, G. X. Gu, Accelerating auxetic metamaterial design with deep learning, *Advanced Engineering Materials* **2020**, 22, 1901266.
- [20] a) B. P. Koya, S. Aneja, R. Gupta, C. Valeo, Comparative analysis of different machine learning algorithms to predict mechanical properties of concrete, *Mechanics of Advanced Materials and Structures* **2022**, 29, 4032; b) M. H. Lim, S. Shin, K. Park, J. Park, S. W. Kim, M. A. Basurrah, S. Lee, D. H. Kim, Deep Learning Model for Predicting Airway Organoid Differentiation, *Tissue Engineering and Regenerative Medicine* **2023**, 20, 1109.
- [21] a) Y. Chang, H. Wang, Q. Dong, Machine learning-based inverse design of auxetic metamaterial with zero Poisson's ratio, *Materials Today Communications* **2022**, 30, 103186; b) X. Sun, L. Yue, L. Yu, C. T. Forte, C. D. Armstrong, K. Zhou, F. Demoly, R. R. Zhao, H. J. Qi, Machine learning-enabled forward prediction and inverse design of 4D-printed active plates, *Nature Communications* **2024**, 15, 5509.
- [22] a) Y. Wang, Q. Zeng, J. Wang, Y. Li, D. Fang, Inverse design of shell-based mechanical metamaterial with customized loading curves based on machine learning and genetic algorithm, *Computer Methods in Applied Mechanics and Engineering* **2022**, 401, 115571; b) M. Wang, S. Sun, T.-Y. Zhang, Machine learning accelerated design of auxetic structures, *Materials & Design* **2023**, 234, 112334; c) S. Bronder, F. Herter, D. Bähre, A. Jung, Optimized design for modified auxetic structures based on a neural network approach, *Materials Today Communications* **2022**, 32, 103931.
- [23] a) C. An, Y. W. Park, S. S. Ahn, K. Han, H. Kim, S.-K. Lee, Radiomics machine learning study with a small sample size: Single random training-test set split may lead to unreliable results, *PLoS One* **2021**, 16, e0256152; b) M. K. Uçar, M. Nour, H. Sindi, K. Polat, The effect of training and testing process on machine learning in biomedical datasets, *Mathematical Problems in Engineering* **2020**, 2020.
- [24] a) A. Tang, J. Ji, J. Li, W. Liu, J. Wang, Q. Sun, Q. Li, Nanocellulose/pegda aerogels with tunable poisson's ratio fabricated by stereolithography for mouse bone marrow mesenchymal stem cell culture, *Nanomaterials* **2021**, 11, 603; b) X. Geng, Y. Yao, H. Huang, Q. Li, L. Wang, Y. Fan, Mechanical and biological characteristics of 3D-printed auxetic structure in bone tissue engineering, *Journal of Biomechanics* **2025**, 184, 112685.
- [25] S. Gohar, G. Hussain, M. Ilyas, A. Ali, Performance of 3D printed topologically optimized novel auxetic structures under compressive loading: experimental and FE analyses, *Journal of Materials Research and Technology* **2021**, 15, 394.
- [26] a) L. Shen, Z. Wang, X. Wang, K. Wei, Negative Poisson's ratio and effective Young's modulus of a vertex-based hierarchical re-entrant honeycomb structure, *International Journal of Mechanical Sciences* **2021**, 206, 106611; b) J. Kang, M. Shirzad, J. M. Seok, W.-K. Jung, S. Y. Nam, Mechanical enhancement of porous scaffolds through integration of auxetic and conventional structures, *Materials Letters* **2025**, 379, 137675.
- [27] T. Almela, I. M. Brook, K. Khoshroo, M. Rasoulboroujeni, F. Fahimipour, M. Tahriri, E. Dashtimoghadam, A. El-Awa, L. Tayebi, K. Moharamzadeh, Simulation of cortico-cancellous bone structure by 3D printing of bilayer calcium phosphate-based scaffolds, *Bioprinting* **2017**, 6, 1.
- [28] a) M. Ekiert, K. A. Tomaszewski, A. Mlyniec, The differences in viscoelastic properties of subtendons result from the anatomical tripartite structure of human Achilles tendon-ex vivo

- experimental study and modeling, *Acta biomaterialia* **2021**, 125, 138; b) M. Kongsgaard, C. Nielsen, S. Hegnsvad, P. Aagaard, S. Magnusson, Mechanical properties of the human Achilles tendon, in vivo, *Clinical biomechanics* **2011**, 26, 772; c) D. Shin, T. Finni, S. Ahn, J. A. Hodgson, H.-D. Lee, V. R. Edgerton, S. Sinha, Effect of chronic unloading and rehabilitation on human Achilles tendon properties: a velocity-encoded phase-contrast MRI study, *Journal of Applied Physiology* **2008**, 105, 1179.
- [29] M. Shirzad, J. Kang, G. Kim, M. Bodaghi, S. Y. Nam, Bioinspired 3D-Printed Auxetic Structures with Enhanced Fatigue Behavior, *Advanced Engineering Materials* **2024**, 2302036.
 - [30] Z. Qi, N. Zhang, Y. Liu, W. Chen, Prediction of mechanical properties of carbon fiber based on cross-scale FEM and machine learning, *Composite Structures* **2019**, 212, 199.
 - [31] S. Kwak, J. Kim, H. Ding, X. Xu, R. Chen, J. Guo, H. Fu, Machine learning prediction of the mechanical properties of γ -TiAl alloys produced using random forest regression model, *Journal of Materials Research and Technology* **2022**, 18, 520.
 - [32] T. Nguyen-Sy, J. Wakim, Q.-D. To, M.-N. Vu, T.-D. Nguyen, T.-T. Nguyen, Predicting the compressive strength of concrete from its compositions and age using the extreme gradient boosting method, *Construction and Building Materials* **2020**, 260, 119757.
 - [33] I. La Fé-Perdomo, J. A. Ramos-Grez, I. Jeria, C. Guerra, G. O. Barrionuevo, Comparative analysis and experimental validation of statistical and machine learning-based regressors for modeling the surface roughness and mechanical properties of 316L stainless steel specimens produced by selective laser melting, *Journal of Manufacturing Processes* **2022**, 80, 666.